Supplementary Materials: Modelling the past and future evolution of tidal sand waves

Janneke Krabbendam [1]*, Abdel Nnafie [1], Huib de Swart[1], Bas Borsje[2] and Luitze Perk[3]

Contents

Introduction

These Supplementary Materials contain 1) a detailed description of the model equations (Text S1); 2) an overview of all boundary conditions used (Text S2); 3) sensitivity of model results to the grid size, morphological acceleration factor (MORFAC), type of boundary conditions and roughness length (Text S3); 4) water levels and velocities obtained with the 2DV sand wave model in comparison with water levels and velocities from ZUNO (Text S4); results regarding the time evolution of crests and troughs (Text S5); 6) a detailed description of the method and the results regarding the effects of different sand transport components (Text S6) and 7) the effects of wind on the residual sand transport (Text S7).

S1. Model equations

S1.0.1. Hydrodynamics

The 2DV shallow water equations in (x,σ)-coordinates are:

$$\frac{\partial u}{\partial t}+u\frac{\partial u}{\partial x}+\frac{\omega}{H+\zeta}\frac{\partial u}{\partial \sigma}=-\frac{1}{g}\frac{\partial \zeta}{\partial x}+\frac{\partial}{\partial x}\left(\nu_H\left(\frac{\partial u}{\partial x}+\frac{\partial u}{\partial \sigma}\frac{\partial \sigma}{\partial x}\right)+\frac{1}{(H+\zeta)^2}\frac{\partial}{\partial \sigma}\left(\nu_V\frac{\partial u}{\partial \sigma}\right)\right) \tag{S1}$$

$$\frac{\partial \omega}{\partial \sigma}=-\frac{\partial \zeta}{\partial t}-\frac{\partial [H+\zeta]u}{\partial x} \tag{S2}$$

Here, u is the horizontal velocity and $\omega=(H+\zeta)D\sigma/Dt$ is the vertical velocity, with D/Dt the material derivative. The gravitational acceleration is denoted by g and ν_H and ν_V represent the horizontal and vertical eddy viscosity coefficients, respectively. The Coriolis effect is not included in the model equations. The bed $(\sigma=-1)$ and the free surface $(\sigma=0)$ are assumed to be impermeable, therefore the vertical velocity ω is set to zero.

The stress at the bed is given by a quadratic friction law, while the stress at the free surface is set to zero:

$$\text{at } \sigma=0: \quad \tau_b=\rho_w\frac{\nu_V}{(H+\zeta)}\frac{\partial u}{\partial \sigma}=0; \tag{S3}$$

$$\text{at } \sigma=-1: \quad \tau_b=\rho_w\frac{\nu_V}{(H+\zeta)}\frac{\partial u}{\partial \sigma}=\rho_w u_*|u_*| \tag{S4}$$

In these equations ρ_w is the water density, τ_b is the bed shear stress, ν_V the vertical eddy viscosity coefficient, u_* the friction velocity and u_b the velocity close to the bed

($u_b = u(\sigma = -1 + \delta)$). The value of δ can be chosen freely, but in this layered σ-model it is chosen as $\frac{1}{2}\Delta\sigma$, i.e. the distance from the middle of the lowest σ-layer to the bed. The vertical structure of the flow near the bed is given by a logarithmic profile:

$$u_b = \frac{u_*}{\kappa} \ln\left(\frac{\sigma + 1}{\sigma_0}\right). \tag{S5}$$

The roughness height in σ-coordinates is σ_0, which is related to the local roughness height z_0 through $z_0 = \zeta + (H + \zeta)\sigma_0$. This local roughness height is related to the Nikuradse roughness height k_s:

$$z_0 = \frac{k_s}{30}. \tag{S6}$$

The value of the Nikuradse height is imposed according Van Rijn [1]:

$$k_s = k_{s,grain} + k_{s,r} + k_{s,mr} \tag{S7}$$

$$= 3d_{90} + 20 l_r d_r \left(\frac{d_r}{\gamma_r}\right) + 1.1\gamma_{mr} d_{mr}(1 - e^{-25 d_{mr}/l_{mr}}) \tag{S8}$$

where d_r and l_r are the height and length of ripples and d_{mr} and l_{mr} the height and length of megaripples, respectively. The constants γ_r and γ_{mr} are form factors, the values of both are γ_r is 0.7 (valid when ripples are superimposed on megaripples or sand waves, otherwise it is 1), the other is set to 1. The dimensions for ripples ($l_r = 0.2$m, $d_r = 0.034$m) originate from Sleath [2] and the megaripple dimensions (l_{mr} = 10 m, d_{mr} = 0.2 m) from Van Dijk et al. [3] and studies by Deltares ([4] and [5]). This results in a Nikuradse roughness height of $k_s = 0.0944 - 0.0949$ m. The Chézy coefficient is then calculated according to [6]

$$C_{3D} = \frac{\sqrt{g}}{\kappa} \ln\left(1 + \frac{\delta}{2z_0}\right). \tag{S9}$$

The $k - \epsilon$-model is chosen as turbulence closure model. This model states that the vertical eddy viscosity coefficient ν_V is related to turbulent kinetic energy k and its dissipation rate ϵ (for a detailed description of this model see [7]). Both k and ϵ are calculated for every point in space and time and used to compute the vertical eddy viscosity $\nu_V = c_\mu \frac{k^2}{\epsilon}$. Here, c_μ is an empirical constant set to 0.09 [6]. The horizontal eddy viscosity ν_H is assumed to be a superposition of an user-defined background eddy viscosity ν_{back} and ν_V, where $\nu_{back} >> \nu_V$ [6]. Here, $\nu_{back} = 1$ m^{2}s^{-1}.

S1.0.2. Bed level evolution

The hydrodynamic results are used to calculate the sand transport with an adaptation of Van Rijn [1], which is the default mode of Delft3D-FLOW. Based on this sand transport, the bed evolution is computed using the sediment continuity equation:

$$(1 - \epsilon_p)\frac{\partial z_b}{\partial t} + \frac{\partial(q_b + q_s)}{\partial x} = 0. \tag{S10}$$

In this equation, ϵ_p is the bed porosity and set to 0.4, and q_b is the magnitude of the bed load transport,

$$q_b = 0.5\alpha_s \rho_s d_{50} u'_* T D_*^{-0.3}, \tag{S11}$$

with α_s the bed slope correction term, ρ_s is the density of the sediment, d_{50} the median sediment grain size and T is the non-dimensional bed shear stress, defined as

$$T = \frac{\mu_c \tau_b - \tau_{b,cr}}{\tau_{b,cr}}. \tag{S12}$$

with $\tau_{b,cr} = (\rho_s - \rho_w) g d_{50} \theta_{cr}$ is the critical bed shear stress for initiation of motion. In this equation θ_{cr} is the critical Shields parameter, which depends on the non-dimensional grain size $D_* = d_{50} \left(\frac{\rho_s - \rho_w}{\nu^2} \right)^{1/3}$. In the range of grain sizes used in this study, θ_{cr} is parametrised as

$$\theta_{cr} = 0.04 D_*^{-0.1}, \tag{S13}$$

with ν is the kinematic viscosity of water. The friction velocity due to currents u'_* is given by

$$u'_* = u_* \mu_c, \tag{S14}$$

where coefficient μ_c takes into account that sediment transport is only the result of skin friction.

$$\mu_c = \frac{f'_c}{f_c}. \tag{S15}$$

This efficiency coefficient is the ratio of the grain-related friction factor f'_c and the current-related friction factor f_c

$$f'_c = 0.24 \left[\log_{10} \left(\frac{12(H+\zeta)}{3 d_{90}} \right) \right]^{-2}, \qquad f_c = 0.24 \left[\log_{10} \left(\frac{12(H+\zeta)}{z_0} \right) \right]^{-2}. \tag{S16}$$

As a last step, the bed load transport is corrected for slope effects in the direction of the current (s-direction) using the formulation of [8]:

$$\alpha_s = 1 + \alpha_{bs} \left(\frac{\tan(\phi)}{\cos(\tan^{-1}(\frac{\partial z_b}{\partial s}))(\tan(\phi) - \frac{\partial z_b}{\partial s})} - 1 \right) \tag{S17}$$

Here, α_{bs} is a user-defined constant, ϕ is the angle of repose of sand set to 30° and $\frac{\partial z_b}{\partial s}$ is the bed slope in the direction of the current.

The magnitude of the suspended load transport is given by the following equation:

$$q_s = \int_{-1+a/(H+\zeta)}^{0} \left(uc - \epsilon_{s,z} \frac{\partial c}{\partial x} \right) d\sigma \tag{S18}$$

Here a is a reference height of $0.01H$, since sediment below this level reacts almost instantaneously to changes in the flow and is therefore considered part of the bed load. The sediment above this height is transported in suspension. The advection-diffusion (mass-balance) for suspended sediment concentration c

$$\frac{\partial (H+\zeta) c}{\partial t} + \frac{\partial [(H+\zeta) cu]}{\partial x} + \frac{\partial (\omega - w_s) c}{\partial \sigma} = (H+\zeta) \frac{\partial}{\partial x} \left(\epsilon_{s,x} \frac{\partial c}{\partial x} \right) + \frac{\partial}{\partial \sigma} \left(\epsilon_{s,z} \frac{1}{(H+\zeta)} \frac{\partial c}{\partial \sigma} \right). \tag{S19}$$

At the free surface ($\sigma = 0$), c is assumed to be zero and at reference height a, the concentration is equal to reference concentration c_a

$$\text{at } \sigma = a: \qquad c = c_a = 0.015 \rho_s \frac{d_{50} T^{1.5}}{a D_*^{0.3}}, \tag{S20}$$

$$\text{at } \sigma = 0: \qquad -w_s c - \epsilon_{s,z} \frac{1}{(H+\zeta)} \frac{\partial c}{\partial \sigma} = 0. \tag{S21}$$

In these equations $\epsilon_{s,z}$ is the vertical eddy diffusivity, which depends on the vertical eddy viscosity ν_V,

$$\epsilon_{s,z} = \frac{\nu_V}{\sigma_c}. \tag{S22}$$

Here, σ_c is the Prandtl-Schmidt number, which is 1 in the case of the k-ϵ turbulence model [6]. The horizontal eddy diffusivity $\epsilon_{s,x}$ is a superposition of the vertical eddy diffusivity and an user-defined background diffusivity such that $\epsilon_{back} \gg \epsilon_{s,z}$,

$$\epsilon_{s,x} = \epsilon_{s,z} + \epsilon_{back}. \tag{S23}$$

The settling velocity w_s depends on the median grain size and is given by

$$w_s = \frac{10\nu}{d_{50}}\left(\sqrt{1 + 0.01D_*^{-3}}\right)^{-1} \tag{S24}$$

S2. Overview of all hydrodynamic boundary conditions

Table S1 presents the amplitudes and phases of U_{grid}, ζ and $R_\pm$ at the lateral boundaries of all four locations. Here, U_{grid} is the depth-averaged velocity component in the direction along the grid. The Riemann constituents are used to obtain the figures, unless explicitly stated otherwise.

Table S1. Boundary conditions imposed at the open boundaries $x = -L/2$ and $x = L/2$.

Loc 1	$x = -L/2$			$x = L/2$		
	U_{grid}	ζ	R_+	U_{grid}	ζ	R_-
$\mathbf{M_2}$	0.62 ms^{-1}, 77°	0.61 m, 68°	1.02 ms^{-1}, 73°	0.66 ms^{-1}, 95°	0.52 m, 120°	0.38 ms^{-1}, 73°
$\mathbf{M_4}$	0.03 ms^{-1}, 90°	0.17 m, 114°	0.14 ms^{-1}, 108°	0.05 ms^{-1}, 166°	0.15 m, 139°	0.06 ms^{-1}, 296°
$\mathbf{M_6}$	0.04 ms^{-1}, 100°	0.02 m, 63°	0.05 ms^{-1}, 92°	0.04 ms^{-1}, 148°	0.05 m, 209°	0.04 ms^{-1}, 89°
$\mathbf{M_0}$	0.001 ms^{-1}	0.02 m	0.02 ms^{-1}	0.01 ms^{-1}	0.02 m	-0.001 ms^{-1}
Loc 2	**South**			**North**		
	U_{grid}	ζ	R_+	U_{grid}	ζ	R_-
$\mathbf{M_2}$	0.73 ms^{-1}, 79°	0.57 m, 49°	1.05 ms^{-1}, 69°	0.62 ms^{-1}, 88°	0.47 m, 104°	0.34 ms^{-1}, 74°
$\mathbf{M_4}$	0.04 ms^{-1}, 58°	0.13 m, 102°	0.11 ms^{-1}, 89°	0.03 ms^{-1}, 130°	0.15 m, 130°	0.07 ms^{-1}, 310°
$\mathbf{M_6}$	0.03 ms^{-1}, 93°	0.03 m, 30°	0.04 ms^{-1}, 68°	0.04 ms^{-1}, 132°	0.03 m, 193°	0.04 ms^{-1}, 100°
$\mathbf{M_0}$	0.04 ms^{-1}	0.02 m	0.05 ms^{-1}	0.007 ms^{-1}	0.02 m	-0.005 ms^{-1}
Loc 3	**South**			**North**		
	U_{grid}	ζ	R_+	U_{grid}	ζ	R_-
$\mathbf{M_2}$	0.65 ms^{-1}, 71°	0.69 m, 63°	1.12 ms^{-1}, 67°	0.65 ms^{-1}, 89°	0.58 m, 107°	0.28 ms^{-1}, 61°
$\mathbf{M_4}$	0.04 ms^{-1}, 75°	0.17 m, 109°	0.15 ms^{-1}, 101°	0.05 ms^{-1}, 150°	0.17 m, 134°	0.08 ms^{-1}, 305°
$\mathbf{M_6}$	0.04 ms^{-1}, 92°	0.03 m, 43°	0.06 ms^{-1}, 78°	0.04 ms^{-1}, 138°	0.05 m, 201°	0.04 ms^{-1}, 88°
$\mathbf{M_0}$	-0.009 ms^{-1}	0.02 m	0.007 ms^{-1}	0.003 ms^{-1}	0.02 m	-0.01 ms^{-1}
Loc 4	**South**			**North**		
	U_{grid}	ζ	R_+	U_{grid}	ζ	R_-
$\mathbf{M_2}$	0.66 ms^{-1}, 54°	0.98 m, 22°	1.16 ms^{-1}, 40°	0.69 ms^{-1}, 75°	0.60 m, 53°	0.36 ms^{-1}, 99°
$\mathbf{M_4}$	0.06 ms^{-1}, 12°	0.10 m, 65°	0.10 ms^{-1}, 38°	0.05 ms^{-1}, 58°	0.14 m, 104°	0.07 ms^{-1}, 316°
$\mathbf{M_6}$	0.02 ms^{-1}, 27°	0.05 m, 346°	0.05 ms^{-1}, 5°	0.03 ms^{-1}, 94°	0.03 m, 30°	0.03 ms^{-1}, 133°
$\mathbf{M_0}$	0.006 ms^{-1}	0.02 m	0.01 ms^{-1}	0.02 ms^{-1}	0.02 m	0.004 ms^{-1}

S3. Sensitivity to model settings

S3.1. Sensitivity to grid size

Figure S1 shows in color the modelled bed level for 2012 for three different grid sizes: $\Delta x = 2.5$ m, $\Delta x = 5$ m (default value) and $\Delta x = 10$ m. Differences between runs with different grid sizes in the area of interest, are on the order of centimeters.

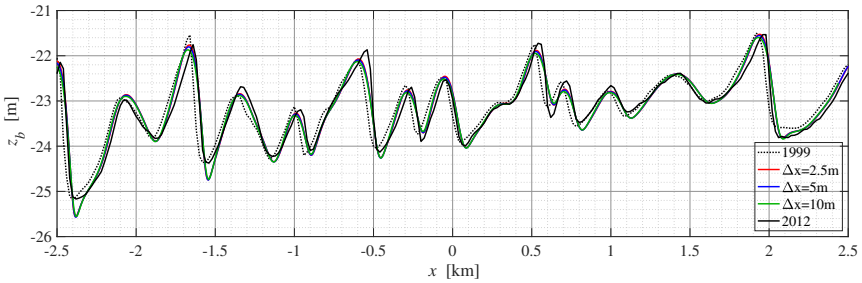

Figure S1. Modelled bed level z_b (m, coloured lines) for 2012 over distance x (km) along transect 1 for different values of grid size Δx. The black dotted line corresponds to initial bed level of 1999 and the black solid line to the bed level of 2012.

S3.2. Sensitivity to MORFAC

Figure S2 shows in color the modelled bed level for 2012 for different value of MORFAC: 37, 74, and 148, the latter of which is the default value. Bed level differences between runs are on the order of a few centimeters.

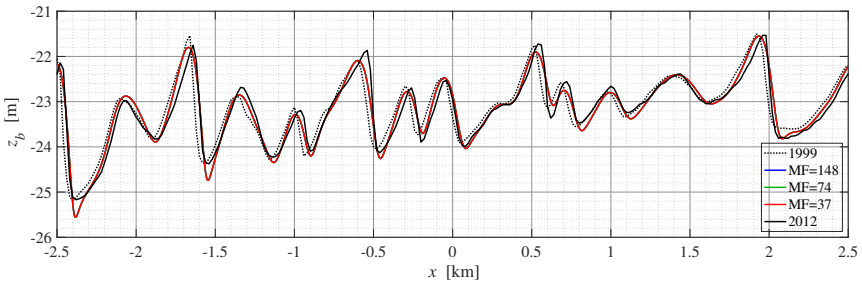

Figure S2. Modelled bed level z_b (m, coloured lines) for 2012 over distance x (km) along transect 1 for different values of MORFAC (MF). The black dotted line corresponds to initial bed level of 1999 and the black solid line to the bed level of 2012.

S3.3. Sensitivity to type of hydrodynamic boundary conditions

Figure S3 shows in color the modelled bed level for 2012 for different types of boundary conditions: RR, RU, UU, UZ, RZ and ZZ. Here, the first letter corresponds to the boundary condition imposed at $x = -L/2$, the second to the one imposed at $x - L/2$. R is Riemann invariant, U stands for depth averaged velocity and Z means water level. Differences in bed levels vary from centimeters to decimeters, differences of the latter magnitude are related to phase differences between the bed levels.

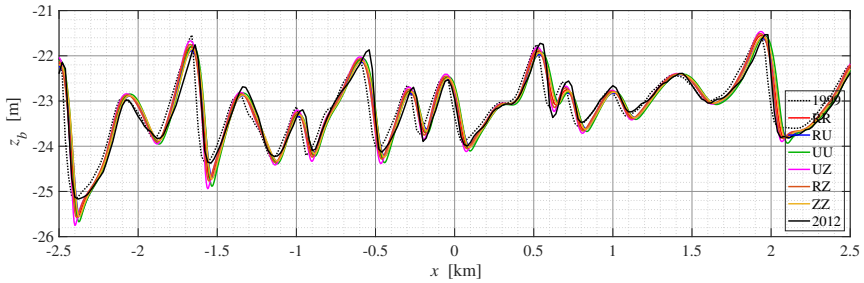

Figure S3. Modelled bed level z_b (m, coloured lines) for 2012 over distance x (km) along transect 1 for different types of boundary conditions. The black dotted line corresponds to initial bed level of 1999 and the black solid line to the bed level of 2012.

S3.4. Sensitivity to roughness length

Figure S4 shows the modelled bed levels for 2012 along transect 1 for megaripple heights $d_{mr} = 0.15,\ 0.2$ and 0.25 m, corresponding to roughness lengths $k_s = 0.06,\ 0.09$ and 0.13 m, respectively. Bed level differences are on the order of centimeters.

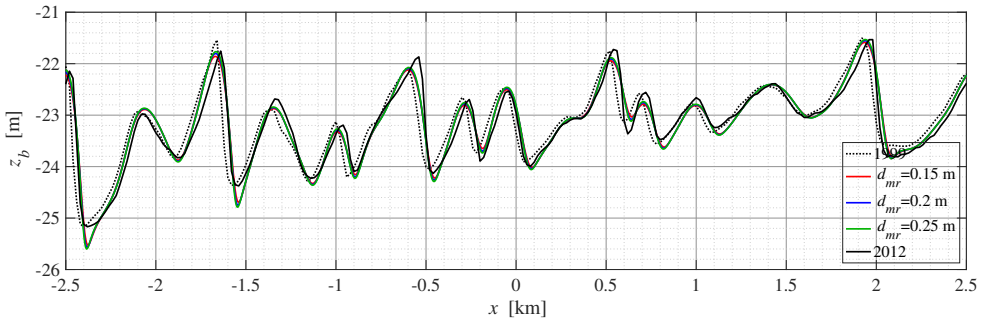

Figure S4. Modelled bed level z_b (m, coloured lines) for 2012 over distance x (km) along transect 1 for different megaripple heights. The black dotted line corresponds to initial bed level of 1999 and the black solid line to the bed level of 2012.

S4. Water levels and velocities

Figures S5 and S6 show the amplitudes and phases of M_2, M_4, M_6 and M_0 depth-averaged velocities (Figure S5) and water levels (Figure S6). The red lines correspond to results obtained with the 2DV sand wave model and the blue lines denote ZUNO output. Each panel matches to one tidal constituent, where the left y-axis relates to the amplitude, which is plotted with solid lines. The RMSE value in the upper left corner is the RMSE value of the 2DV amplitude with respect to the amplitude from ZUNO. The right y-axis denotes the phase and corresponds to the dashed lines. The RMSE value in the upper right corner is the RMSE value of the 2DV phase with respect to the phase from ZUNO.

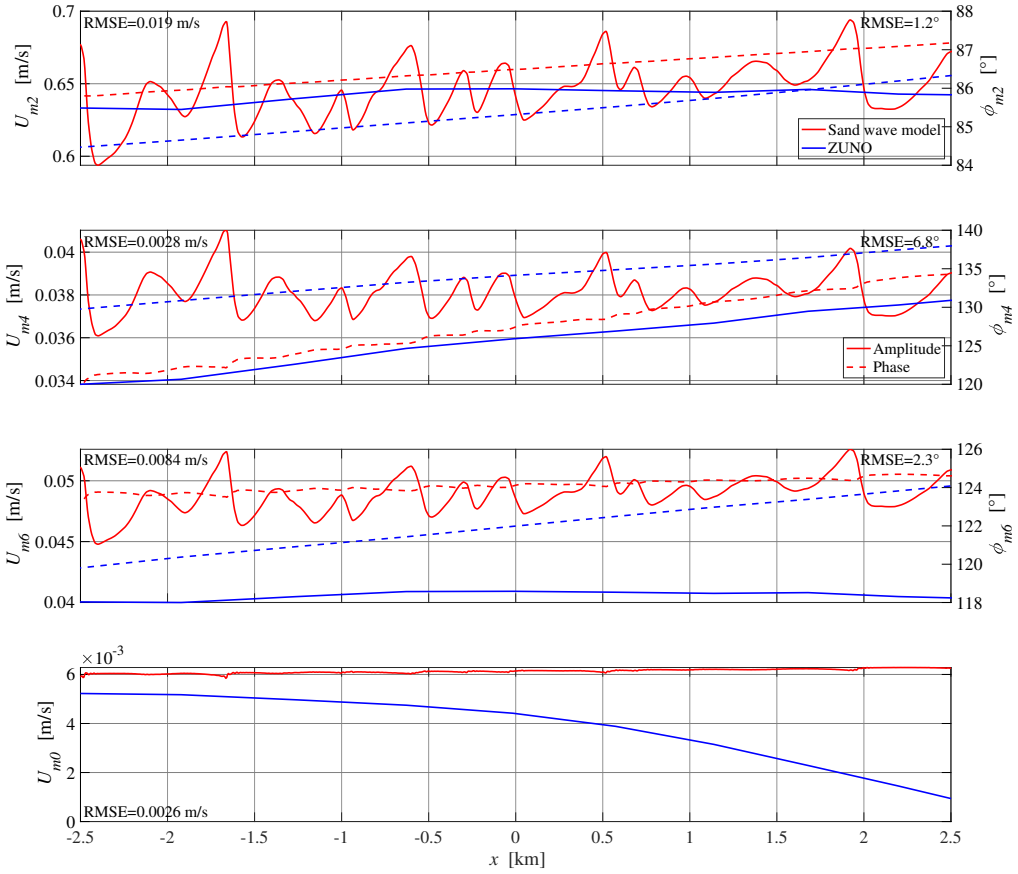

Figure S5. Amplitude and phase of depth averaged velocity of M_2 (**a**), M_4 (**b**), M_6 (**c**) and M_0 (**d**). The red lines correspond to results obtained with the 2DV sand wave model and the blue lines denote ZUNO output. The left y-axis denotes the amplitude (m/s), which corresponds to the solid lines. The RMSE value in the upper left corner is the RMSE value (m/s) of the 2DV amplitude with respect to the amplitude from ZUNO. The right y-axis denotes the phase (°) and corresponds to the dashed lines. The RMSE value in the upper right corner is the RMSE value (°) of the 2DV phase with respect to the phase from ZUNO.

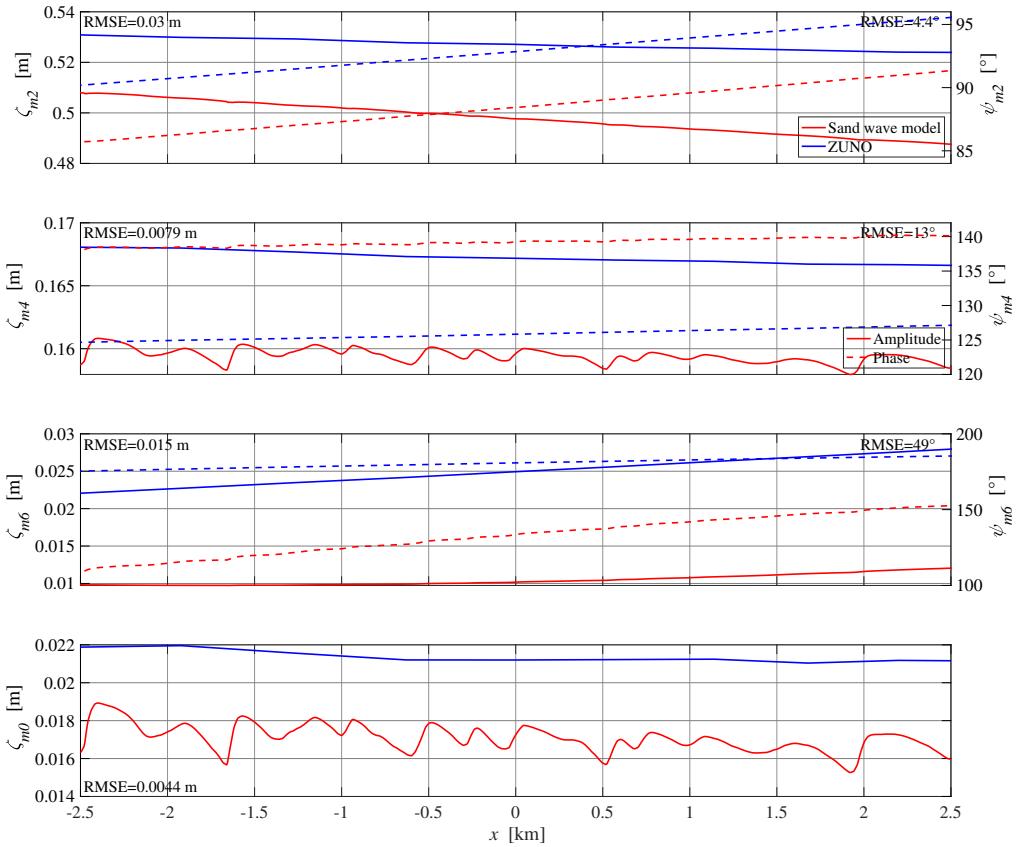

Figure S6. Amplitude and phase of water level of M_2 (**a**), M_4 (**b**), M_6 (**c**) and M_0 (**d**). The red lines correspond to results obtained with the 2DV sand wave model and the blue lines denote ZUNO output. The left *y*-axis denotes the amplitude (m), which corresponds to the solid lines. The RMSE value in the upper left corner is the RMSE value (m) of the 2DV amplitude with respect to the amplitude from ZUNO. The right *y*-axis denotes the phase (°) and corresponds to the dashed lines. The RMSE value in the upper right corner is the RMSE value (°) of the 2DV phase with respect to the phase from ZUNO.

S5. Time evolution of crests and troughs

Figure S7 shows in colours the time evolution of two crests and troughs along transects 1 (**(a)** and **(b)**) and 2 (**(c)** and **(d)**). The initial location is indicated with a coloured scatter in Figures S7 **(a)** and **(c)**. This colour matches to the lines in Figures S7**(b)** and **(d)**, which show the evolution over time of these crest heights and trough depths during the hindcast simulation. Figure S8 shows the same, but then for transects 3 and 4.

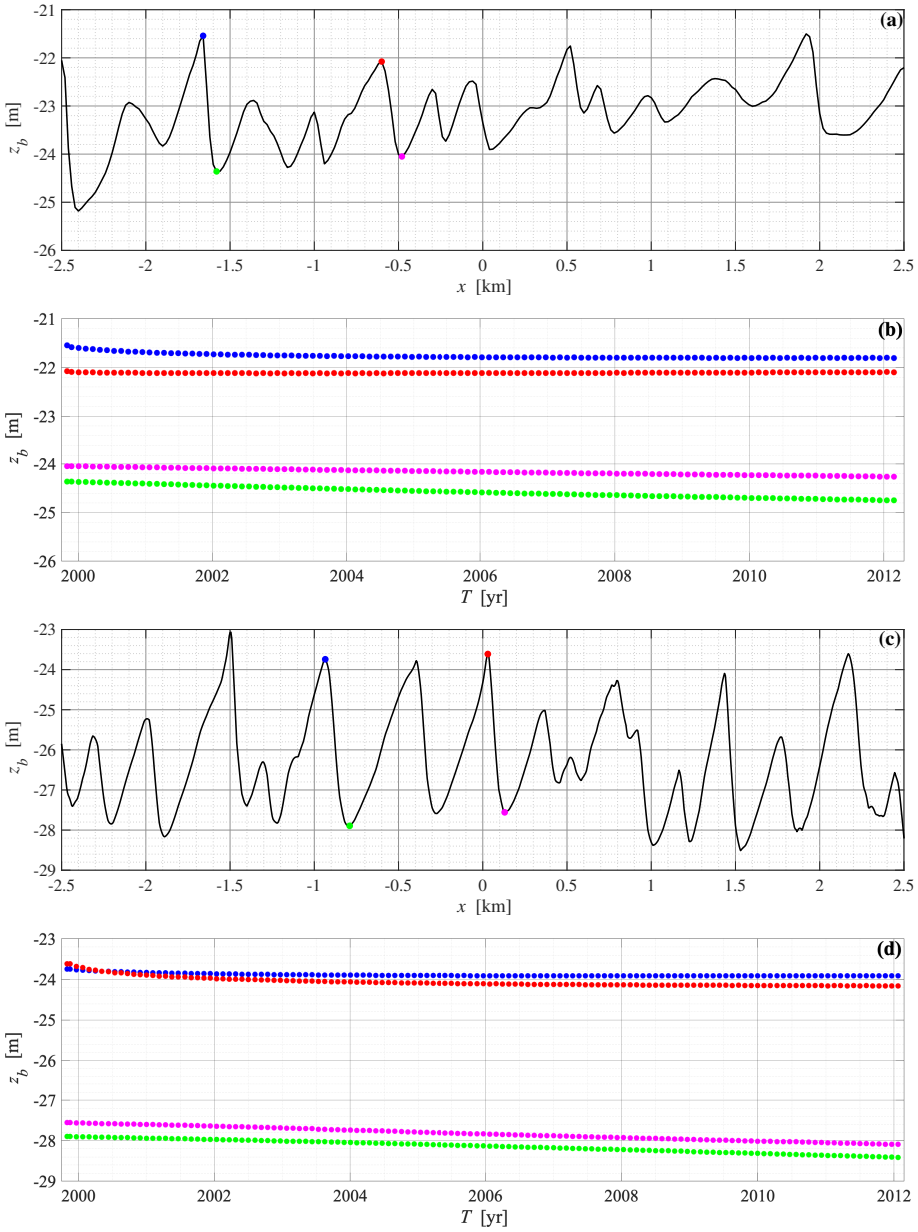

Figure S7. (a) and **(c)** show the initial, measured bed levels z_b (m) along transects 1 and 2. The coloured scatters correspond to the lines in panels **(b)** and **(d)** which show the evolution of the height of these crests and troughs over time along transects 1 and 2, respectively.

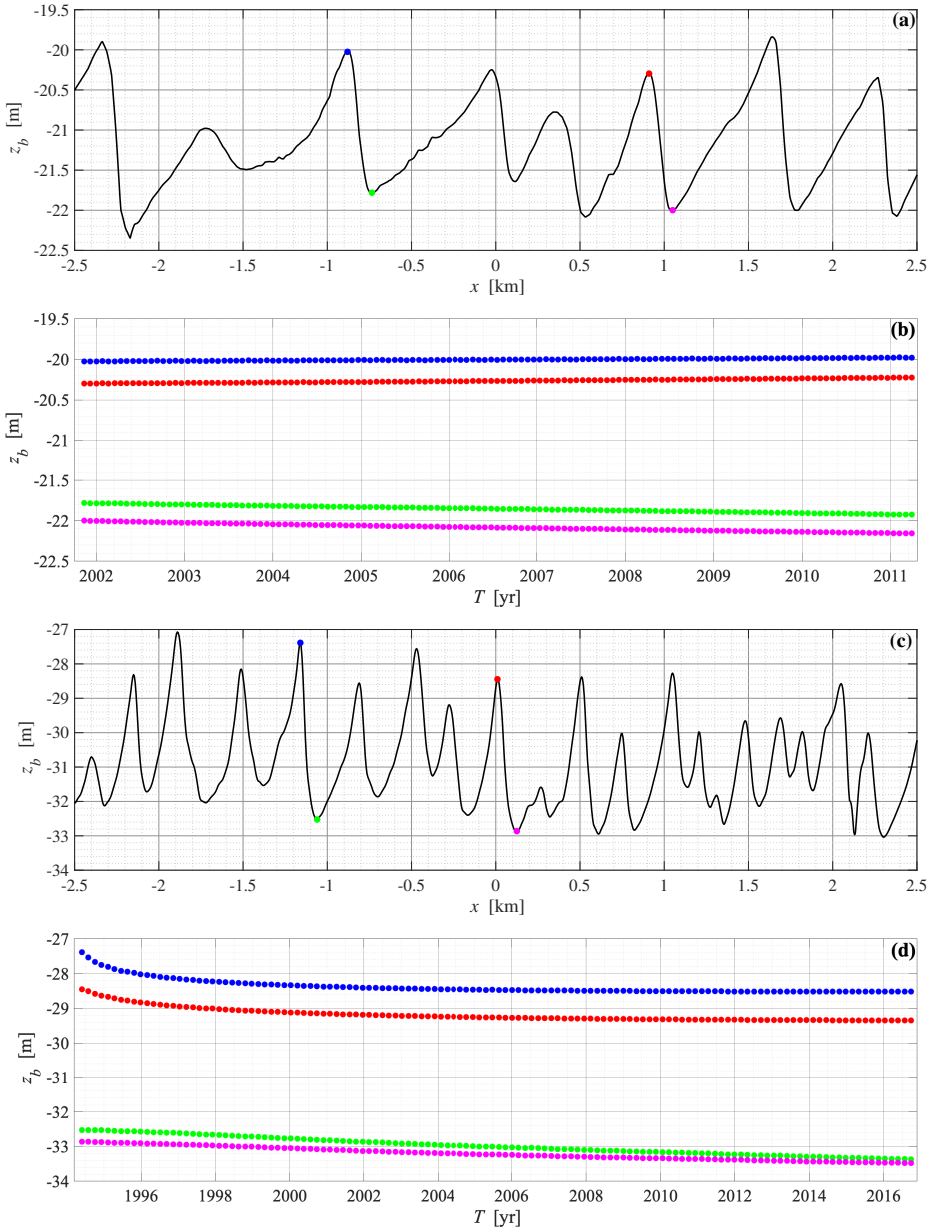

Figure S8. (a) and **(c)** show the initial, measured bed levels z_b (m) along transects 3 and 4. The coloured scatters correspond to the lines in panels **(b)** and **(d)** which show the evolution of the height of these crests and troughs over time along transects 3 and 4, respectively.

S6. Effect of different components of sand transport

S6.1. Methodology

Two types of runs were performed: (1) runs with $\alpha_{bs} = 5.5$ and (2) runs with $\alpha_{bs} = 0$. This first type computes the total bed load transport $q_b(x,t)$, the second type only the advective part of the bed load transport $q_{b,adv}(x,t)$. The bed load transport due to slope effects is defined as the difference between the two: $q_{b,slope}(x,t) = q_b(x,t) - q_{b,adv}(x,t)$. The suspended load transport $q_s(x,t)$ is unaffected by the value of α_{bs}.

The runs are forced with tidal components M_2, M_4, M_6 and M_0, but these are imposed with 12 hour, 6 hour and 4 hour periods, respectively, so that the transports can be averaged over exactly n tidal cycles to compute the residual sand transport:

$$\langle q_i \rangle = \frac{1}{nT} \int_0^{nT} q_i(x,t) dt \tag{S25}$$

with i the component of the transport, $n = 6$ and $T = 12$ h. Then the divergence of each of the components of the sand transport is computed, which in this 2DV case is equal to the gradient in the x-direction: $\frac{\partial \langle q_i \rangle}{\partial x}$. Bed level perturbations h are defined as deviations from the mean bed level:

$$h = z_b - \overline{z_b} \tag{S26}$$

here, z_b is the full bed level and the bar denotes a spatial mean over the area of interest (i.e. $\frac{1}{\ell} \int_{-\ell/2}^{\ell/2} \cdot \, dx$). The root mean square bed level perturbations h_{rms} are defined as:

$$h_{rms} = \left(\overline{h^2}\right)^{1/2} \tag{S27}$$

With the use of the sediment continuity equation, the bed level changes resulting from each of the sand transport components can be computed

$$\frac{\partial h_i}{\partial t} = -\frac{1}{1-p} \frac{\partial \langle q_i \rangle}{\partial x} \tag{S28}$$

with p the bed porosity set to 0.4. Now all ingredients are present to compute the global growth rate σ (s^{-1}) in the same way as Garnier et al. [9]:

$$\sigma_i = \frac{1}{h_{rms}^2} \overline{\left(h \frac{\partial h_i}{\partial t} \right)} \tag{S29}$$

The global migration rate V (m s^{-1}) is computed using the expression suggested by Vis-Star et al. [10]:

$$V_i = -\frac{1}{\overline{\left(\frac{\partial h}{\partial x}\right)^2}} \overline{\frac{\partial h}{\partial x} \frac{\partial h_i}{\partial t}} \tag{S30}$$

S6.2. Results

Figure S9 shows the divergence of the residual sand transport components calculated over a bed level 5 years after start of the run at transects 2 and 4. This is calculated in the exact same way as the transports over the initial bed level as shown in Figure 8 of the main text, but then for a bed level 5 years after the start of the morphological simulation.

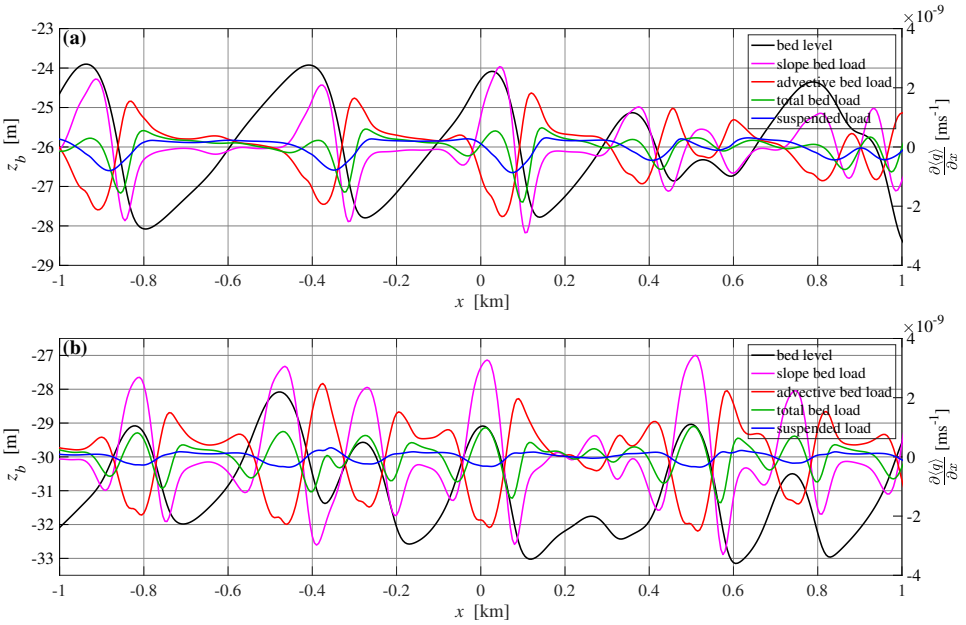

Figure S9. Horizontal gradient of tidally averaged sand transport $\frac{\partial\langle q\rangle}{dx}$ (m/s) over distance along transect x (km) for slope related bed load transport (magenta), advective bed load transport (red), total bed load transport (green) and suspended load transport (blue). Transports are calculated for a bed level 5 years after start of the morphological simulations along transect 2 **(a)** and transect 4 **(b)**.

S7. Effects of wind on sand transport

Figure S10 shows the divergence of the residual sand transport components along transect 1 for the case with and without wind. Here, panel **(a)** corresponds to a uniform and constant wind forcing of U_{10} = 8 m/s coming from the southwest (225°, nautical convention), and for panel **(b)** the direction was changed to 45°.

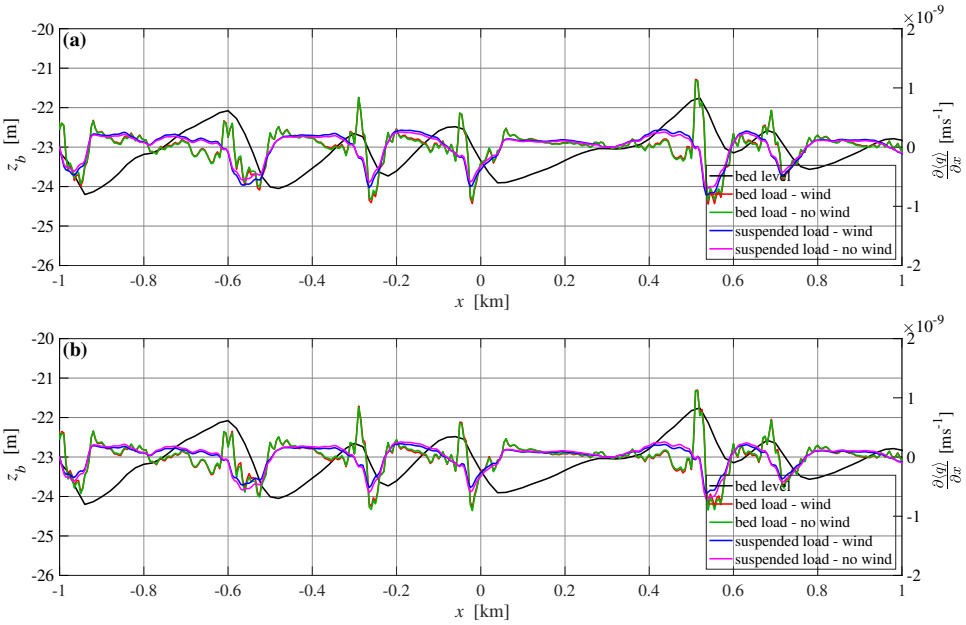

Figure S10. Horizontal gradient of tidally averaged sand transport $\frac{\partial\langle q\rangle}{dx}$ (m/s) over distance along transect x (km) for bed load transport in case of wind (red), bed load transport without wind (green), suspended transport in case of wind (blue) and suspended load transport without wind (magenta). Wind is imposed with U_{10} = 8 m/s and direction of 225° **(a)** and 45° **(b)**. Wind directions are used in nautical convention.

References

1. Van Rijn, L.C. *Principles of sediment transport in rivers, estuaries and coastal seas*; Aqua publications Amsterdam, 1993. doi:10.1002/9781444308785.
2. Sleath, J.F. *Sea bed mechanics*; Wiley, United States, 1984. (ed. M. E. McCormick).
3. Van Dijk, T.A.; Kleinhans, M.G. Processes controlling the dynamics of compound sand waves in the North Sea, Netherlands. *J. Geophys. Res.: Earth Surf.* **2005**, *110*, 1–15. doi:10.1029/2004JF000173.
4. Paulsen, B.T.; Roetert, T.; Raaijmakers, T.; Forzoni, A.; Hoekstra, R.; Van Steijn, P. *Morphodynamics of Hollandse Kust (zuid) Wind Farm Zone, report 1230851-000-HYE-0003*; Deltares, Delft, 2016.
5. Raaijmakers, T.; Roetert, T.; Bruinsma, N.; Riezebos, H.J.; Van Dijk, T.; Forzoni, A.; Vergouwen, S.; Grasmeijer, B. *Morphodynamics and scour mitigation for Hollandse Kust (noord) Wind Farm Zone, report 11202796-000-HYE-0002* ; Deltares, Delft, 2019.
6. Deltares. *Delft3D 3D-FLOW user manual, version: 3.15.34158*; Deltares, Delft, 2014.
7. Burchard, H.; Craig, P.D.; Gemmrich, J.R.; van Haren, H.; Mathieu, P.P.; Meier, H.E.; Smith, W.A.M.; Prandke, H.; Rippeth, T.P.; Skyllingstad, E.D.; Smyth, W.D.; Welsh, D.J.; Wijesekera, H.W. Observational and numerical modeling methods for quantifying coastal ocean turbulence and mixing. *Prog. Oceanogr.* **2008**, *76*, 399–442. doi:10.1016/j.pocean.2007.09.005.
8. Bagnold, R.A. *An approach to the sediment transport problem from general physics, in US Geological Survey Professional Paper 422-I*; U.S. Government Printing Office, Washington, D.C., 1966; pp. 1–37. doi:10.3133/pp422I.
9. Garnier, R.; Calvete, D.; Falqués, A.; Caballeria, M. Generation and nonlinear evolution of shore-oblique/transverse sand bars. *J. Fluid Mech.* **2006**, *567*, 327–360. doi:10.1017/S0022112006002126.
10. Vis-Star, N.C.; De Swart, H.; Calvete, D. Patch behaviour and predictability properties of modelled finite-amplitude sand ridges on the inner shelf. *Nonlin. Processes Geophys.* **2008**, *15*, 943–955. doi:10.5194/npg-15-943-2008.